Low dose rate γ-irradiation protects *Drosophila melanogaster* chromosomes from double strand breaks and telomere fusions by modulating the expression of the esi-RNA biogenesis factor *Loquacious*.

Porrazzo A.[1,3], Cipressa F.[2,3], De Gregorio A.[1], De Pittà C[4]., Sales G. [4], Ciapponi L.[1], Morciano P.[5], Esposito G.[6,7], Tabocchini M.A.[7], Cenci G.[1,3,*]

1. Dipartimento di Biologia e Biotecnologie "C. Darwin". Sapienza Università di Roma, Rome, Italy
2. Centro Studi e Ricerche ''Enrico Fermi'', Rome, Italy
3. Fondazione Cenci Bolognetti/ Istituto Pasteur Italia, Rome, Italy
4. Dipartimento di Biologia, Università di Padova, Padua, Italy
5. INFN-Laboratori Nazionali del Gran Sasso, 67100 Assergi, Italy
6. Istituto Superiore di Sanita` (ISS, Rome, Italy)
7. INFN-Roma 1 (Rome, Italy)

ORCID AP 0000-0002-2914-7984
ORCID GS 0000-0003-2078-5661
ORCID GE 0000-0002-8751-1895
ORCID FC 0000-0002-9919-5295
ORCID CDP 0000-0001-8013-8162
ORCID MAT 0000-0003-3244-6106
ORCID PM 0000-0002-8101-0096
ORCID GC 0000-0002-9628-1411
ORCID LC 0000-0002-0817-1862
ORCID ADG 0000-0002-6560-293X

*Corresponding Author:

Giovanni Cenci, giovanni.cenci@uniroma1.it

Running Title: Low dose rate γ irradiation and chromosome integrity

Abstract

It is still continuously debated whether the low-dose/dose-rate (LDR) of ionizing radiation represents a hazard for humans. Model organisms, such as fruit flies, are considered valuable systems to reveal insights into this issue. We found that, in wild-type *Drosophila melanogaster* larval neuroblasts, the frequency of Chromosome Breaks (CBs), induced by acute γ-irradiation, is significantly reduced when flies are previously exposed to a protracted dose of 0.4Gy delivered at a dose rate of 2.5mGy/h. This indicates that this exposure, which is associated with an increased expression of DNA damage response proteins, induces a radioadaptive response (RAR) that protects Drosophila from extensive DNA damage. Interestingly, the same exposure reduces the frequency of telomere fusions (TFs) from Drosophila telomere capping mutants suggesting that the LDR can generally promote a protective response on chromatin sites that are recognized as DNA breaks. Deep RNA sequencing revealed that RAR is associated with a reduced expression of *Loquacious D (Loqs-RD)* gene that encodes a well-conserved dsRNA binding protein required for esiRNAs biogenesis. Remarkably, loss of *Loqs* mimics the LDR-mediated chromosome protection as it decreases the IR-induced CBs and TF frequency. Thus, our molecular characterization of RAR identifies Loqs as a key factor in the cellular response to LDR and unveils unprecedented epigenetic routes involved in radioresistance.

Introduction

Low doses and low dose rates of ionizing radiation constitute one of various types of genotoxic stresses to which all living organisms are continuously exposed during their daily life. Human exposure to low dose/dose rates radiation depends on both natural (i.e. radon gas, terrestrial radiation and cosmic rays that penetrate the Earth's atmosphere) and man-made (i.e. such as X-rays, radiation used to diagnose diseases and for cancer therapy and fallout from nuclear explosives testing) sources. Low doses are defined as doses lower or equal to 0.1 Gy and low dose rates are defined as dose rates lower or equal to 0.1 mGy/min (that is 6 mGy/h) for low LET radiation [1]. Whereas there is no doubt that intermediate and high doses of ionizing radiation, delivered either acutely or during a prolonged period, have deleterious effects in humans, including, but not exclusively, cancer and developmental defects, the biological consequences at lower doses (below 100mGy) are less clear [2, 3]. Yet, the comprehension of low doses radiation risks has societal importance considering the concerns arising from occupational radiation exposure, screening tests for cancer, nuclear power generation, frequent-flyer risks, missions in space, and radiological terrorism. Several efforts have been made to evaluate the effects of low doses/low dose rate radiation from epidemiological studies. However, these studies are influenced by several uncertainties that include, but not limited to the radiation quality, the age at exposure, the effects of both internal and external exposures, gender and temporal factors [2, 3]. Thus, to better assess the accuracy of risk estimates and increase the statistical power, the low dose/low dose rate epidemiological studies would require a large population to be analyzed or pooling of data from several observations.

The linear-no-threshold (LNT) model has long been used for setting dose limitations on radiation exposure, that is, basically assuming that all radiation exposures, regardless of how low the dose is, increase the risk for cancer [4]. The justification of using this model is that radiation carcinogenesis is triggered by DNA damage. Yet, the possibility of improving the LNT risk extrapolation model has been recently debated as other potential mechanisms affecting radiation carcinogenesis have been described [5-7]. These include epigenetic mechanisms, transmissible genome instability, bystander effects, radiation hormesis and Radio Adaptive Response [3, 8].

The Radio Adaptive Response (RAR) is a protective phenomenon where a small initial low radiation dose (priming) reduces the response to a subsequent high radiation dose (challenging). The main proposed mechanisms to explain RAR are an increase of

the efficiency of DNA repair activity and of the level of antioxidant enzymes [9-11]. First discovered in cultured human lymphocytes [12], RAR has been observed both *in vivo* and *in vitro* in several mammalian systems as well as in the zebrafish embryo model using various end points such as cell lethality, chromosomal aberrations, mutation induction and DNA repair [9, 10]. Although the general view posits that RAR may be due to enhanced repair of DNA damage in the " primed" cells (those having exposed to a priming dose) when compared to the " unprimed" cells, several experiments using different cell types and irradiation procedures produced conflicting results [13]. Thus, our understanding on the molecular mechanisms that underlie RAR is still elusive. Indeed, the manifestation of the response depends on several factors such as the cell, tissue, animal types, genetic background, p53 status. Moreover, the dose, dose rate and time period between priming and challenging dose may be crucial for a cell to induce RAR. It is still unclear what dose and dose rate might trigger RAR in humans [3, 11]. This is also complicated by the high degree of inter-individual variation, which in turn depends on the radio-sensitivity of an individual. Thus, the evaluation of whether low radiation doses or dose rates represent a risk estimate factor for radiation protection purposes requires a better understanding of the RAR.

Recently, a link between radiation protection and telomere maintenance has emerged. The examination of leukocytes in atomic bomb survivors of Hiroshima revealed a long-term detrimental effect of an inverse correlation between telomere length and IR dose [14]. Effects on telomere length have also been observed during space mission as cosmic radiation has been shown to elongate telomeres. Interestingly, two days on the Earth restored normal telomere length indicating that elongation of telomeres can be considered as a well-established adaptive response to high radiation levels in space [15, 16]. Nevertheless, exposure to high radiation background does not affect telomere length suggesting the existence of a well-defined threshold under which the effects of radiation exposure are undetectable [17, 18].

Here we show that Drosophila larvae that are chronically exposed to a specific priming γ-radiation dose of 0.4Gy delivered at 2.5mGy/h (0.4Gy LDR) during embryo-to-third instar larvae development, exhibit a strong reduction of chromosome break frequency after a 10Gy γ ray challenging dose, with respect to non-pretreated flies. Moreover, we demonstrate that the same LDR treatment reduces the frequency of telomeric fusions (TFs) associated with the loss of telomere capping suggesting that the 0.4Gy LDR-mediated protective effect can be generally extended to chromatin sites that are also

inappropriately recognized as DNA breaks. Deep RNA sequencing indicates that the 0.4Gy LDR-mediated protective effect on chromosome breaks is associated with a reduction of the Loquacious D (Loqs-PD) isoform, a well conserved dsRNA binding protein required for the esiRNA biogenesis. Interestingly, loss of Loqs PD (but not of other isoforms) reduces IR-induced DSBs and TFs indicating that modulation of Loqs PD may represent an escape route for the cell to preserve chromosome integrity upon induction of genotoxic stress.

Results

A 2.5mGy/h dose rate gamma irradiation protects Drosophila chromosomes from ionizing radiation-induced chromosome damage.

To investigate the effects of low dose rate irradiation on chromosome damage, we assessed whether a pretreatment with chronic low doses of γ rays (priming dose) affects the frequency of total chromosome breaks (CBs; for examples of CBs see Figure 1a) induced by an acute γ dose of 10Gy (challenging dose) in Drosophila third instar larvae neuroblasts. Vials containing 12h old Drosophila embryos were placed at 23 °C inside the LIBIS irradiation facility [19] and irradiated continuously at a dose rate of 2.5mGy/h until they developed into third instar larvae (7 days for a final dose of 0.4Gy, herein 0.4Gy LDR). Irradiated and non-irradiated control vials were then exposed to a challenging dose, at the dose rate of about 0.7Gy/min, and four hours later larval neuroblasts were analysed for CBs frequency (Supplementary Figure 1). Chromosomes were fixed at 4h and 8h post irradiation time points (PIR) to recover cells that were irradiated in the S-G_2 or G_1 stage, respectively [20]. The average number of total chromosome breaks per cell (CBs/cell) was calculated by measuring the ratio of the total number of chromatid deletions (CDs, scored as a single event) and isochromosome breaks (ISOs or chromosome deletions, scored as two events) to the total number of metaphases (Figure 1b). Cytological analysis of exposed pretreated and non-pretreated third instar larvae showed that in non-pretreated larvae the average number of CBs/cell induced by the challenging dose after 4h PIR was ~1.0 in females and and ~ 0.8 males. Differently, the 0.4Gy LDR determined a ~2 fold decrease of CBs/cell frequency in both male and female larval neuroblasts, indicating that the LDR treatment renders neuroblast chromosomes resistant to IR-induced DNA breakage as result of the activation of radioadaptive response (RAR). Interestingly, a 1.2mGy/h dose rate for 7 days (0.2Gy total dose) was not sufficient to trigger a RAR, suggesting that this response could be dose rate dependent (Supplementary Figure 2a).

We sought to understand whether the 0.4Gy LDR could affect CBs frequency also at 8h PIR, when cells are irradiated during the G_1 stage. The analysis of ~1000 female metaphases revealed no statistically significant difference on CBs frequency between non-pre-treated (54%) and 0.4Gy LDR treated (45%) larvae at 8h PIR (Figure 1b). This suggests that 0.4Gy LDR could primarily influence the HR-based repair systems that, by employing sister chromatids as templated DNA synthesis to regenerate the sequence surrounding the break site, is restricted to S-G_2 phase [21]. Furthermore, we evaluated

whether the radiation resistance could be also maintained for more than one generation. Thus, male and female adult flies that developed from 0.4Gy LDR-pretreated larvae were mated to each other outside the LIBIS and the resulting F_1 larvae irradiated with 10Gy. Interestingly, we found that the frequency of CBs, calculated at 4hr PIR, was ~2 fold reduced in metaphases from both male and female F_1 larvae of 0.4Gy LDR -derived adult parents (n=1900 for both sexes) with respect to control F_1 larvae deriving from non-pretreated adults (Figure 1b). This indicates that the RAR shows a transgenerational inheritance. However, the F_1 obtained from reciprocal crossings between 0.4Gy LDR-treated females or males and non-treated males or females, respectively, did not elicit RAR (Supplementary Table 1), suggesting that the transgenerational inheritance of RAR depends on both maternal and paternal factors.

To analyze whether the 0.4Gy LDR affected the regulation of G_2/M checkpoint, we carried out a standard checkpoint assay evaluating the proportion of dividing cells (Mitotic Index, MI) in larval brain cells fixed at different times after the challenging dose (10Gy). As shown in Figure 2a, the MI of the non-pretreated Oregon R control brains dropped at 5–30 min PIR, remained low for 1 h and came back to a normal value only at 2 h PIR. The MI of 0.4Gy LDR -pretreated larvae decreased as much as in control brains at 5-30 min PIR, but then markedly increased after 30 min PIR, suggesting that the 0.4Gy LDR exposure determined a faster recovery from the G_2-M checkpoint (Figure 2a) compared to non-pretreated cells, most likely due to a reduced amount of DNA damage (~50%) to be repaired.

We also checked whether the rate of IR-induced apoptosis was influenced by the 0.4Gy LDR. Immunostaining of whole-mounted brains and imaginal discs for cleaved-Caspase-3 revealed that the number of positive cells in treated larval brains was indistinguishable from that observed in non-pretreated control after the challenging dose, indicating that RAR does not reduce the occurrence and distribution of apoptosis caused by extensive DNA damage (Supplementary Figure 3a-d). We finally compared the occurrence of DNA replication in non-pretreated and pretreated brain cells by analyzing the incorporation of the EdU (5-ethynyl-2'-deoxyuridine) analog of thymidine, before and after IR (see Materials and Methods). Before 10Gy irradiation, non-pretreated wild-type and 0.4Gy LDR-pretreated larvae, exhibited a similar proportion of nuclei (~14%; n= ~2000 cells) that were actively replicating their DNA and incorporated EdU. However, after irradiation, whereas in non-pretreated wild-type brains the frequency of EdU-labeled nuclei dropped to 6.5% (as a consequence of the arrest of S phase), 0.4Gy LDR-pretreated

brains displayed a proportion of positive nuclei (~20%; n= ~2000 cells) very similar to unirradiated larvae (Figure 2c). Based on the EdU incorporation pattern, according to Cenci et al., 2015 [22], we subdivided the S phase in three subclasses, namely S_1 (early/mid S; nucleus partially or completely stained with the exception of the chromocenter), S_2 (mid/late S; staining at the chromocenter and at a less compacted nuclear area) and S_3 (late S; only chromocenter stained; Figure 2b). This classification revealed us that pretreated and non-pretreated cells did not differ in the relative frequencies of nuclei showing S_1, S_2 and S_3 EdU incorporation patterns (Figure 2d). Altogether, these results indicate that 0.4Gy LDR-pretreated cells recover much faster than non-pretreated controls from the DNA damage-induced replication block.

The RAR to chromosome aberrations relies on a more efficient DNA damage response

To determine whether the reduction of chromosome breaks promoted by 0.4Gy LDR depends on the presence of proteins required for specific DSB repair pathways, we checked whether 0.4Gy LDR-pretreated larvae bearing mutations in genes encoding DSB repair master proteins (dATM, dRad50, dNbs1, dMre11), HR-specific repair proteins required for resection or homology search and strand invasion (dRad51, Bloom), and NHEJ-specific proteins (ligase IV, Ku70) elicited a decrease of CBs frequency after the challenging dose. The analysis of mitotic chromosomes from all mutants revealed no significant difference ($p<0.05$) in the frequency of CBs between 0.4Gy LDR-pretreated and non-pretreated larvae, indicating that the 0.4Gy LDR-mediated resistance to γ-ray-induced CBs is strictly dependent on DNA repair genes (Figure 2e).

We then verified whether 0.4Gy LDR affects the kinetics of γH2Av recruitment to chromatin breaks. H2Av is the functional homolog of H2AX in Drosophila and its phosphorylation at Ser147 is induced by DSB [23]. 0.4Gy LDR -pretreated and non-pretreated larvae were exposed to 10Gy γ rays and then checked by IF for the presence of γH2Av foci in larval neuroblasts (Figure 3a) after 5 min, 15 min, 30 min and 60 min PIR. We found that in non-pretreated control larval brains, the number of γH2Av foci/cell progressively increased over the time, reached the highest peak (6 foci/cell) at 30 min PIR and started to slowly decrease at 60 min PIR (Figure 3b). LDR -pretreated neuroblasts also showed a progressive increment of the γH2Av foci/cell frequency over the time with a peak at 30 min PIR. Interestingly, the average of foci/cell at 30 min was around ~4 indicating that, differently from non-pretreated controls, LDR-pretreated brains accumulate

less damage, most likely as the results of either an accelerated DNA damage response or a more efficient DNA repair (Figure 3b). We have also analyzed the kinetics of γH2Av accumulation by WB and found that, consistently with our IF results, at 30 min PIR γH2Av in 0.4Gy LDR-pretreated cells does not accumulate as robustly as in non-pretreated cells (Figure 3c,d), confirming that 0.4Gy LDR could accelerate the completion of the DNA damage response. We also analyzed the levels of the MRN complex as well as of Ku70 in both pretreated and non-pretreated cell extracts. WB analyses revealed a statistically significant increase of Rad50 and Nbs1, but not of Ku70, protein levels in 0.4Gy LDR-pretreated cells with respect to non-pretreated cells (Figure 3e,f). Collectively these data, along with the genetic analyses indicating a strict requirement of DNA repair genes, suggest that the RAR relies on an efficient DNA damage response. However, we cannot rule out the possibility that the LDR could also influence chromatin compaction making it more reluctant to damage or more accessible to DNA repair factors compared to non-pretreated chromatin.

LDR protects chromosomes from telomere dysfunction.

We also asked whether other DNA damage-induced events are also affected by LDR. We focused on DNA damage response elicited by dysfunctional telomeres and verified the occurrence of telomere fusions (TFs) in mutants with a defective telomere capping. Depletion of either terminin complex components and or terminin-associated factors induces the formation of multicentric linear and ring chromosomes very likely because of NHEJ-mediated fusion events that occur at uncapped telomeres [24, 25] (for examples of TFs see Figure 4a). We thus measured the frequency of TFs of 0.4Gy LDR-pretreated mutants in selected genes coding for telomere capping proteins, such as *verrocchio (ver)* and *caravaggio (cav)* that specify the terminin proteins VER and HP1-ORC-Associated Protein (HOAP), or *Su(var)205, pendolino (peo)* and *effete (eff)* that encodes the non terminin protein Heterochromatin Protein 1a (HP1), Peo and UbcD1, respectively [24, 25]. As indicated in Figure 4b, we found that in all mutants analyzed, 0.4Gy LDR yielded a significant reduction of TFs indicating that this exposure exerts a protective effect at uncapped chromosome ends. We have also analyzed the frequency of TFs caused by mutations in *tefu, nbs, rad50* and *mre11* genes encoding for the DNA repair factors ATM, Nbs, Rad50 and Mre11, respectively and which are also required for protecting telomeres from fusion events [26, 27]. Interestingly, we found that the frequency of TFs in DNA repair mutants was indistinguishable from that of non-pretreated mutants

(Figure 4b) indicating that, similarly to RAR, the 0.4Gy LDR-induced telomere protection depends on DNA repair factors. However, the reduction of TFs did not always correlate with a reduction of γH2Av-positive Telomere Induced Foci (TIF) indicating that, unlike chromosomal DSBs, the reduction of fusigenic feature or uncapped telomeres has not a direct effect on the cytological detection of telomere damage (Supplementary Figure 4a,b). We finally checked if LDR could induce an increase of retro-transposition of the telomeric retroelement HeT-A, as it occurred in flies that were chronically exposed to sub-lethal doses of paraquat [28]. RT-qPCR analysis revealed no differences in the HeT-A expression between non-pretreated and 0.4Gy LDR treated TF mutants (Supplementary Figure 4c), indicating that the 0.4Gy LDR protective effects on uncapped telomeres is unlikely due to an adaptive role of telomere elongation against the loss of capping.

Differential Gene Expression and Genetic Analyses reveal Loquacious (Loqs) as a RAR responsive factor.

To assess whether the 0.4Gy LDR RAR was accompanied by differential modulation of specific set of genes, we performed a genome wide RNA-seq analysis of total RNAs extracted from unirradiated (A), 10Gy- (B), 0.4Gy LDR- (C) and 0.4Gy LDR + 10Gy-irradiated (D) larval male brains. To search for gene functions specifically associated to the chromosome break phenotype, RNAs of 10Gy- and 0.4Gy LDR + 10Gy irradiated larvae were extracted from brains dissected after 4h following the acute dose exposure. Pairwise comparisons revealed that the 0.4Gy LDR treatment *per se* has not determined a statistically significant modulation of general levels of transcripts compared to the unirradiated condition. In contrast, both 10Gy- and 0.4Gy LDR + 10Gy-treatments yielded a moderate, yet statistically significant, modulation of transcription in all comparisons (see Supplementary Tables 3-7 for a list of both upregulated and downregulated genes). The Venn diagram including all differentially expressed genes (DEGs) from 0.4Gy LDR + 10Gy *vs.* 10Gy, 0.4Gy LDR + 10Gy *vs*. 0.4Gy LDR and 10Gy *vs*. 0.4Gy LDR comparisons, has shown only a small number of genes in common among all comparisons (Figure 5a). To further identify genes potentially involved in the RAR, we focused on the set of DEGs found in the 0.4Gy LDR + 10Gy *vs*. 10Gy comparison (D *vs*. B). DAVID functional enrichment analysis (EASE score < 0.05, Adjusted p-value <0.05) revealed that the DEGs from this comparison are involved in RNA processing (see Heat Map of Figure 5b). 3 genes *(l(3)72Ab, CG5205 and CG8064)* were also differentially expressed in the 0.4Gy LDR + 10Gy vs 0.4Gy LDR comparison.

Among these unique genes, we have drawn our attention to the modulation of *loqs (loquacious)* transcripts that encode the dsRNA binding protein Loqs, which is required for siRNA and micro-RNA biogenesis and that is the fly homolog of mammal TRBP [29, 30]. Four different transcripts have been identified for *loqs* (*loqs-RA*, *loqs-RB, loqs-RC* and *loqs-RD)* that give rise to the Loqs-PA, Loqs-PB, Loqs -PC and Loqs –PD isoforms, respectively. Loqs-PA and Loqs-PB,~~,~~ interact with Dcr-1 during miRNA biogenesis [30-33]. Loqs-PC is rarely expressed and has no known function [30] while Loqs-PD facilitates Dcr-2–dependent endosiRNA biogenesis [30, 31]. Our RNA-Seq experiment showed that the *loqs-RD* (but not the other transcripts) appeared ~2 fold decreased in 0.4Gy LDR + 10Gy samples compared to 10Gy irradiated samples. This reduction was also validated by RT-qPCR on three independent RNA extractions (Figure 6a) suggesting that LDR could specifically influence Loqs-dependent esi-RNA biogenesis. Consistent with this, we found that 0.4Gy LDR + 10Gy larvae showed a statistically significant increase of *mus308* transcripts that are the endogenous targets of *esi-1* RNA [34], with respect to both unirradiated and 10Gy irradiated larvae (Figure 6a). Moreover, we analyzed the effect of 0.4Gy LDR + 10Gy on the eye color of *GMR-w^{IR}* flies, which express an inverted repeat dsRNA (IR-dsRNA) only in the eyes and that show a white eye phenotype when the RNAi pathway is functional [35]. We compared the eye color of LDR-pretreated *GMR-w^{IR}* flies with that of un-pretreated *GMR-w^{IR}* flies upon 10Gy irradiation and found that LDR treated flies exhibited dark orange eyes while eyes from the un-pretreated *GMR-w^{IR}* flies were white (Figure 6b,c). Finally, *Loqs-RD* levels did not change in larvae exposed to 1.2mGy/h dose rate and that did not elicit RAR (Supplementary Figure 2b). Thus, we concluded that RAR is associated with reduction of Loqs-PD activity and consequently of esi-RNA biogenesis.

To further understand whether the reduction of Loqs indeed accounts for the RAR, we analyzed chromosome integrity in chronically irradiated Loqs-depleted larval brain cells with and without the 0.4Gy LDR-treatment. We thus measured the frequencies of CBs in the *loqs^{KO}* null mutant upon 0.4Gy LDR, 10Gy and 0.4Gy LDR +10Gy treatments as well as in unirradiated *loqs^{KO}* brains using the same experimental set up described above. Intriguingly, we found that while unirradiated *loqs^{KO}* larval brain cells exhibited very rare CBs, the frequency of CBs in this mutant was >50% reduced with respect to Or-R control larvae (n= 250) after the exposure to 10Gy (Figure 6d). This suggests that the depletion of Loqs could mimic the effect of the 0.4Gy LDR priming dose in determining resistance to ionizing radiation-induced CBs. Interestingly, we observed that this response was lost when Loqs-PD, but not –PB, was expressed in the *loqs^{KO}* null mutant (Figure 6d),

confirming that only the reduction of this specific isoform is involved in triggering radio-resistance to CBs. However, we observed that the >50% reduction of CB frequency in 10Gy irradiated *loqs*^{KO} null mutant, did not further decrease upon the 0.4Gy LDR pretreatment, suggesting that the effect of Loqs loss on the radio-resistance is epistatic over the 0.4Gy (2.5mGy/h) LDR priming dose (Figure 6d). Finally, we observed a ~50% reduction of CBs also in *loqs*^{KO}/+ heterozygotes, suggesting that radioresistance effect is dominant and confirming our RNA-seq data that even a moderate downregulation of this gene can account for the protection against extensive DNA breakage.

To confirm that the loss of Loqs mirrors the effects of the 0.4Gy LDR -induced radio-resistance, we first verified whether the response to CBs in Loqs-depleted cells is also dependent on DNA repair factors. We thus sought to analyze CB frequency in *loqs*^{KO}*; tefu*^{atm} and *loqs*^{KO}*; nbs*^{1} double mutants. While *loqs*^{KO}*; tefu*^{atm} double mutants turned out to be early lethal, thus preventing us for a further characterization, we found that the frequency of CBs in 2Gy irradiated *loqs*^{KO}*; nbs*^{1} larvae was similar to that of 2Gy irradiated *nbs*^{1} single mutants (Supplementary Table 2), confirming that the protection from chromosome breakage in Loqs-depleted and 0.4Gy LDR cells requires shared DNA protein factors. Finally, we observed that the kinetics of γH2Av recruitment in *loqs*^{KO} and in 0.4Gy LDR + 10Gy cells, were similar (Figure 6e). Altogether, this set of evidences confirms that repression of Loqs explains the LDR-mediated RAR and endorses the view that Loqs-PD is *a bona fide* low dose responsive gene.

Loss of Loqs reduces the frequency of Telomere Fusions in Drosophila telomere capping mutants.

We then sought to verify if a reduction of Loqs, similarly to LDR, affects the fusigenic ability of chromosomes with defective telomere capping. We thus checked the frequency of TFs in double mutant combinations between *loqs*^{KO} and TF mutants (*ver*^{1}*, cav*^{1}*, nbs*^{1}*)* mapping on the third chromosome and therefore more suitable for recombination with *loqs*^{KO}, located on the second chromosome. Very interestingly, we found that in *loqs*^{KO} *; ver*^{1} and *loqs*^{KO} *; cav*^{1} mutant combinations the percentage of TFs/cell was significantly lower than that observed in the corresponding controls, while, as expected, TF frequency of *nbs1* mutants was not affected by loss of Loqs (Figure 6f). This finding further confirms that, similarly to RAR, the reduction Loqs is also involved in the protection of uncapped telomeres.

Discussion

We showed for the first time that a protracted exposure to LDR protects Drosophila chromosomes from IR-induced DSBs in mitotic cells, by promoting a more efficient DNA damage response. Our genetic and cytological characterizations indicated that this response, dubbed RAR, is enhanced when DSBs occur after DNA replication and depends on both HR and NHEJ DNA repair pathways, which are normally activated during the S-G_2 checkpoint [36]. We also found that RAR is associated to increased levels of the Rad50 and Nbs proteins but not of Ku70, suggesting that the upregulation of MRN complex could play a pivotal role in the LDR-promoted DNA repair. However, it cannot be excluded that other components of either HR or NHEJ pathway could be differentially regulated as a consequence of RAR, a point that deserves further in-depth analyses as soon as more antibodies against Drosophila DNA repair factors will be made available. We also demonstrated that LDR reduces also the frequency of TFs of *Drosophila* capping mutants, revealing an unprecedented protective effect on dysfunctional chromosome ends. Since Drosophila has emerged as a well established model organism for human telomere biology [25, 37], we can envisage that our findings could provide a valid countermeasure to inhibit telomere fusions in cancer cells. It can be argued that the reduction of TFs mediated by the 0.4Gy LDR, which enhances DNA repair, could appear in contradiction with the evidence that telomeres normally avoid unwanted DNA repair [38]. However, it is also known that DNA repair proteins interact with telomere capping proteins to establish a protective structure during G_2-M [38-40]. We can thus hypothesize that the 0.4Gy LDR could reinforce the DNA repair protein recruitment that has been impaired by the loss of capping factors, thus counteracting telomere dysfunction/fusions. The findings that some Drosophila capping proteins indeed interact with the MRN complex [41, 42] and that loss of either ATM or MRN induces TFs [37], gives further support to this hypothesis. Interestingly, the observation that the frequency of TFs associated to depletion of either ATM or MRN is not affected by 0.4Gy LDR provides a robust evidence that, similarly to the RAR, the protective effect on uncapped telomeres is dependent on the activation of DNA-damage response. Thus, our results indicate that the protective effects of LDR on CBs and TFs share common molecular bases.

Our total RNA seq analyses revealed that mRNA profile of “primed” cells is undistinguishable from that of “unprimed” cells before the induction of DSBs indicating that the 0.4Gy LDR *per se* has no effect on gene expression. However, we cannot exclude that LDR could change the expression of small non-coding RNAs, such as microRNAs.

Furthermore, 0.4Gy LDR does not seem to affect life parameters as 0.4Gy LDR treated flies are fertile and do not exhibit changes in the life span (Supplementary Figure 4). However, compared to unprimed cells, the induction of DSBs in primed cells yielded a discrete modulation of gene transcription, which might help understand the molecular bases underlying the LDR protective effects. Our evidence that the downregulation of *loqs-RD* transcript is required to prevent extensive chromosome breakage in primed cells could suggest a link between esiRNAs biogenesis and radio adaptive response. Remarkably, we found that depletion of *loqs-RD,* similarly to 0.4Gy LDR, confers radio-resistance to mitotic chromosomes upon DSBs induction, confirming that the downregulation of this dsRNA binding protein can account for the 0.4Gy LDR-mediated response to DNA damage. In light of this, we can certainly state that *loqs-RD* can be considered the first 0.4Gy LDR-responsive gene ever characterized. In addition, we would like to point out that an understanding of the molecular basis of RAR could help identify unanticipated factors involved in radioresistance.

Loqs-PD interacts with Dicer-2 through its C-terminal region, and is crucial for efficient production of subset of siRNAs, namely hairpin-derived endo-siRNA, cis-Natural Antisense Transcript (NAT)-derived endo-siRNA, as well as exo-siRNAs generated from an inverted repeat transgene [43]. However, Loqs-PD is not essential for the production of transposon-derived endo-siRNAs and virus-derived exo-siRNAs [44]. Locus-specific siRNA formation has been observed associated to DSBs in different systems, including flies [45-47] and promoting repair by HR in mammalian cells and plants [46, 48]. However, as the inactivation of siRNA pathways does not result in DNA repair defects in flies, the significance of siRNA formation in Drosophila DNA repair remains unaddressed [49]. Thus it is plausible to consider that endogenous siRNAs derived from cis-antisense transcripts as well as from other dsRNA sources that are normally converted to siRNA by Loqs-PD, do not play a direct role in DNA repair thus explaining why *loqs* mutants do not elicit defects in DNA repair. It is also plausible that Loqs-PD could influence DNA repair independently of its involvement in siRNA biogenesis or that the accumulation of esiRNA precursors could account for a more proficient DNA damage response. Yet, given the high level of homology between Loqs-PD and its human counterpart TARBP2/PACT, it would be extremely interesting to evaluate in the future whether TARBP2/PACT could also induce protective effects on human chromosomes.

Materials and Methods

Drosophila strains

The mutations in DNA repair genes *mei41*^{29D}, *rad50*$^{\Delta 5.1}$, *mre11*^{DC}, *nbs*^{1}, *tefu*^{atm6} and in telomere capping genes *cav*^{1}, *moi*^{1}, *ver*^{1}, *Su(var)205*^{05}, *eff*^{tre2}, *peo*^{h}, and *peo*^{1} were previously described [22, 50-57] The mutant stocks *lig4*^{5} (Bl#8519), *rad51*^{1}*/SpnA1* (Bl#3322), and *loqs*^{KO} (Bl#65411) were obtained from the Bloomington Stock Center. The mutant stock ku70^{EX8} was obtained from W. R. Engels (University of Wisconsin, Madison, WI), the *GMR-w*^{IR} transgenic line from Carine Meignin (University of Strasbourg, France). The *loqs*^{KO} ; *[loqs-PA]*, *loqs*^{KO} ; *[loqs-PB]* and *loqs*^{KO} ; *[loqs-PD]* lines were a generous gift from P. Zamore (University of Massachusetts Medical School, Worcester, MA). The *Oregon* R strain was used as a control in all experiments. All strains were maintained at 25 °C on *Drosophila* medium (Nutri-Fly®GF; Genesee Scientific) treated with propionic acid. The detailed information on the balancers and the genetic markers used are available online on Flybase (http://flybase.bio.indiana.edu/).

Irradiation treatments

All the irradiations were carried out at the Istituto Superiore di Sanità (ISS, Rome, Italy). For the chronic γ ray treatment 12 hours embryos from 20 young females mated to 20 young males were irradiated at the LIBIS γ-irradiation facility with ^{137}Cs sources (Esposito et al., 2016). The 0.4 Gy LDR and the 0.2 Gy priming doses were chronically delivered with a dose rate of 2.5 mGy/h and 1.2 mGy/h, respectively during embryo to third instar development (7 days at 25°C). For the RAR analysis, chronically exposed third instar larvae were irradiated with 10, 5 and 2Gy γ rays (challenge dose) from ^{137}Cs sources, at a dose rate of 0.7 Gy/min using the Gammacell Exactor 40 (Nordion). Following irradiation, non-irradiated and irradiated flies were maintained in the same incubator at 25°C.

Eye color quantification

For quantification of eye color, heads were detached from thoraxes of 20 females after freezing in liquid nitrogen, and rapid vortexing. Heads were then incubated one day at 25°C in 1 ml of a 30% ethanol solution, pH 2 and the eye pigment was analyzed with a spectrophotometer at 480 nm [58]

Chromosome cytology and microscopy

DAPI (4,6-diamidino-2-phenylindole)-stained, colchicine-pretreated *Drosophila* larval brain chromosome preparations for the analysis of chromosome aberrations and telomere fusions were obtained as previously described [57]. Briefly, larval brains were dissected in NaCl 0.7% and treated for 1 hour with 10^{-6} M colchicine. Successively, they were transferred in a hypotonic solution (0.5% sodium citrate), and then they were fixed in 45% acid acetic, squashed on the slides, and immediately frozen in liquid nitrogen. After the removal of coverslips, the slides were stained with DAPI/VECTASHIELD® (VECTOR Laboratories). At least 150 metaphases for each condition were analyzed through direct observation using the inverted fluorescence microscope Nikon TE 2000 (Nikon Instruments Inc., Americas) equipped with a Charged-Coupled Device (CCD camera; Photometrics CoolSnap HQ).

Immunostaining and γH2Av foci detection

To evaluate the IR-induced γH2Av foci kinetics of recruitment to DNA damage sites, brains from irradiated third instar larvae were dissected and fixed at various post-irradiation times (PIR). The samples were incubated in 3.7% formaldehyde for 5 minutes, transferred for 30 seconds in 45% acetic acid, and fixed in 65% acetic acid. Successively, the brains were squashed and frozen in liquid nitrogen. After the removal of the coverslips, the slides were placed in cold ethanol for 15 minutes, rinsed for 15 minutes in 0.1%TritonX-100/PBS (PBT), and incubated with the anti-γH2Av primary antibody diluted in PBT (1:10; Mouse; Developmental Studies Hybridoma Bank, IA 52242) overnight at 4°C. Then, all slides were incubated with the fluorescein (FITC)-conjugated AffiniPure Donkey Anti-Mouse IgG (H+L) (1:150; Jackson ImmunoResearch) for 1 hour at room temperature (RT). Immunostained preparations were mounted in VECTASHIELD® Antifade Mounting Medium containing DAPI (4,6 diamidino-2-phenylindole) (VECTOR Laboratories). To quantify the foci at least 1000 cells were analyzed for each PIR. The slides were analyzed using a Zeiss Axioplan epifluorescence microscope (Carl Zeiss, Obezkochen, Germany) equipped with a cooled CCD camera (Photometrics, Woburn, MA, USA). The digital images in grayscale were acquired separately, converted in photoshop format, RGB stained, and merged.

EdU incorporation and staining

EdU labeling was performed as previously described [22] using the ClickiT Alexa Fluor 488 Imaging kit (Invitrogen). Brains of third instar larvae were treated with 10 mM EdU for 60

minutes and then fixed and analyzed as described above. To quantify the EdU-positive cells, at least 2000 cells were analyzed for each condition. For the statistical analysis, two different experiments were performed.

Apoptosis levels analysis

Wing imaginal discs and brains were dissected from third instar *Oregon*-R larvae in NaCl 0.7% after 8-10 hours following the acute exposure with 10 Gy. The samples were placed in 4% formaldehyde diluted in PBS 1X for 20 minutes and then permeabilized in 1%Triton-100/PBS for 15 minutes. The samples were incubated with the anti-Cleaved *Drosophila* Dcp-1 (1:50; Rabbit; Asp216 #9578; Cell Signaling Technology®) overnight at 4°C. The next day, the slides were incubated with the AlexaFluor® 488 AffiniPure Donkey Anti-Rabbit IgG (H+L) (1:300; Jackson ImmunoResearch) for 30 minutes After a further wash of 15 minutes in PBT, the samples were stained with DAPI and mounted on the slides. The slides were analyzed using the inverted fluorescence microscope Nikon TE 2000 (Nikon Instruments Inc., Americas) equipped with a Charged-Coupled Device (CCD camera; Photometrics CoolSnap HQ). The digital images in grayscale were acquired separately, converted in photoshop format, RGB stained, and merged. The analysis of digital pictures was performed using ImageJ 1.8.0 (Image Processing and Analysis in Java).

Antibody Generation.

To obtain the anti-Ku70 antibody, rabbits were immunized with a 6×His-tagged C-terminal polypeptide of Ku70 encompassing amino acids 1–256 (UniProtKB Q23976 KU70_DROME). The resulting antisera were affinity-purified by standard methods. Rabbit immunization and antisera affinity purification were carried out by Agro-Bio (La Ferté St Aubin, France).

Protein extracts and Western blotting

Protein extracts from Drosophila larval brains were obtained by dissecting 10 larval brains in 0.7% NaCl and homogenizing them in 20 μl of 2X Laemmli buffer. Protein samples were loaded into a 4-20% Mini-PROTEAN TGX precast gel to perform electrophoresis (SDS-PAGE) and blotted using the Trans-Blot® Turbo™ Transfer System on a nitrocellulose membrane (Hybond ECL, Amersham). Filters were blocked in 5% non-fat dry milk dissolved in 0.1% Tween-20/PBS for 30 min at RT and, then, incubated with anti-Giotto

(1:5000; Rabbit; [59]) and anti-γH2Av (1:1000; Mouse; Developmental Studies Hybridoma Bank, IA 52242) overnight at 4°C. The membranes were then incubated with HRP-conjugated anti-Mouse and anti-Rabbit IgGs secondary antibody (1:5000; Amersham) for 1 hour at RT and then washed again 3 times with 0.1%Tween-20/PBS. The chemiluminescent signal was revealed through either SuperSignal™ West Femto or SuperSignal™ West Pico substrate (Thermo Scientific™) using the ChemiDoc scanning system (Bio-Rad). Band intensities were quantified by densitometric analysis using the Image Lab 4.0.1 software (Bio-Rad). WB was repeated independently at least three times.

Genomic DNA extraction and RT-qPCR

To evaluate *Het-A* abundance, DNA was extracted from third instar larvae by standard procedures. The amount of *Het-A* was assessed by RT-qPCR using the following primers:

*Het-A*_FW 5'-ACCATAATGCCAACAGCTCC-3'
*Het-A*_RV 5'-AGCCAGCATTGCAGGTAGTT-3'

The Reference gene used was *RP49* (see below).

Total RNA extraction and RNA seq

Drosophila RNA was isolated from brain of third instar larvae exposed to four different irradiation treatments (non-pretreated control, 0.4 Gy chronic exposure, 10 Gy acute exposure, and 0.4 Gy + 10 Gy). Brains (100 brains/sample) were dissected in triplicate and RNA extracted using TRIzol (TRI Reagent® SIGMA Life Science, Sigma-Aldrich). The RNA-Seq of each individual sample was carried out from IGA Technology Services (Udine, Italy). cDNA libraries were constructed with 1 µg of total RNA by using the "Ovation® Drosophila RNA-Seq System" (TECAN-NuGEN, Redwood City, CA, USA) following the manufacturer's instructions. The total RNA was fragmented 3 min at 94 °C. 1X Agencourt AMPure XP beads (Agencourt Bioscience Cooperation, Beckman Coulter, Beverly, MA, USA). Total RNA samples and final cDNA libraries were quantified with the Qubit 2.0 Fluorometer (Invitrogen, Carlsbad, CA, USA) and quality tested by Agilent 2100 Bioanalyzer Nano assay. For cluster generation on the flow cell, libraries were processed with cBot (Illumina, San Diego, CA, USA) following the manufacturer's instructions. Sequencing was carried out in single-end mode (1×75 bp) by using NextSeq500 (Illumina) with a targeted sequencing depth of about 40 million reads per sample. Raw data were

processed with the software CASAVA v1.8.2 (Illumina) for both format conversion and de-multiplexing. Resulting reads were trimmed to remove adapter sequences using cutadapt (version 1.15) and then analyzed using the bcbio-nextgen pipeline (version 1.0.6). Specifically, reads were aligned against the Drosophila melanogaster reference genome (BDGP6) using STAR (v2.5.3a); gene abundances were estimated with Salmon (v0.9.1). Differential expression analysis at the gene level was performed using the DESeq2 R package. Genes with an adjusted p-value (FDR) <0.05 after correction for multiple testing (Benjamini-Hochberg method) were considered differentially expressed. lncRNAs polyA+ were also detected as the RNAseq library was polyA+ enriched. Finally, to analyze the functional relationships of these differentially expressed genes, a Gene Ontology (GO) functional enrichment analysis through the DAVID v. 6.8 web tool (https://david.ncifcrf.gov/,[60]) was performed.

Sequence reads are available on NCBI BioProject database with the accession number SUB10002092

cDNA amplification and qPCR

To validate the expression levels of transcripts selected from the RNA seq analysis, equal amounts of cDNA were synthesized from 300 ng of total RNA for each sample by using the iScript™ cDNA Synthesis Kit (Bio-Rad, Hercules, CA, USA). Thirty nanograms of cDNA per reaction were analyzed for semi-qPCR using the SsoAdvanced™ Universal SYBR® Green Supermix Kit (Bio-Rad) following the manufacturer's protocol. The thermal cycling conditions were: 50 °C (2 min), 95 °C (10 min) followed by 40 cycles at 95 °C (15 s), 60 °C (1 min), and 95 °C (15 s), 60 °C (1 min) 95 °C (15 s), and 60 °C (15 s). The specificity of the reaction was verified by melting curve analysis. The PCR primers used were:

loqsRD_FW 5'-GCAAGGGCAAAAGCAAGAAGA-3'
loqsRD_RV 5'-TTGAATGATACTCACTTCGCCCT-3'

loqsRB_FW 5'-ACTGCTTAAGTTACAGAAGA-3'
loqsRB_RV 5'-GGCCAGAGAAGGTCTTCTCC-3'

loqsRA/RE_FW 5'-GTCTGCAGGAGACTCCCATC-3'
loqsRA/RE_RV 5'-TCAAGCAAGTTTCGCCCTCC-3'

mus308_FW 5'-AGCGGACGACAAGGAGAATG-3'
mus308_RV 5'-GGAGAACTCGTCCCGGAAAA-3'

rp49 was amplified as a reference transcript using the following primers:

rp49_FW 5'-CCGCTTCAAGGGACAGTATCT-3'
rp49_RV 5'-ATCTCGCCGCAGTAAACGC-3'

PCR reactions were carried out in the ABI Prism 7300 System (Applied Biosystems, Foster City, CA, USA). Data processing was performed using the ABI SDS v2.1 software (Applied Biosystems). The critical threshold value was noted for each transcript and normalized to the internal control. The fold change was calculated using the comparative $2^{(-\Delta\Delta Ct)}$ method (Livak and Schmittgen, 2001).

Statistical analysis

Data were presented using the mean ± standard error (SE) obtained from, except for the EdU analysis, at least three independent experiments. All the statistical analyses were performed with Sigmaplot 11.0 (Systat Software, Imc., Chicago, IL, USA). The comparison between the two groups was analyzed by the Student t-test. The results were considered statistically significant when the *p* values were <0.05.

Acknowledgments

We are grateful to Prof. P.D Zamore (University of Massachusetts Medical School) for sharing all *loqs* transgenic flies. We thank P. Anello (ISS, Rome, Italy) for technical assistance with the γ irradiators. This work has been supported by grants from the Institute Pasteur of Paris (PTR-24-2017), and Institute Pasteur of Rome to GC, by grants from FERMI Institute for Multidisciplinary Studies (Cosmic Silence Project, Italy), INFN-CSN5 (RENOIR experiment) and ISS-INFN Operative Agreement for R&D activities in the field of Radiobiology to MAT

Figure legends

Figure 1. Effects of 0.4Gy LDDR treatment on CBs.

(a) Examples of IR-induced CBs in neuroblasts from O*regon*-R third instar larvae. (A) Wild type female and (D) male metaphases; (B) female and (C; F) male metaphases with examples of isochromosome breaks (arrows); (E) male metaphase showing autosomal chromatid deletions (arrows). Bar= 5μm. **(b)** Analysis of the frequency of CBs induced by the acute exposure to 10Gy, in 0.4Gy LDR chronically treated and non-treated (NT) larvae after 4 and 8h post irradiation (PIR), and in the first and the second generation from adults exposed to 0.4Gy LDR during their development. Chromosome exchanges did not vary and were not considered in the analysis. At least three independent experiments were conducted. Error bars represent the standard errors of the mean. LDR: low dose rate; ISOs: isochromosome deletions; CDs: chromatid deletions; CBs: chromosome breaks; PIR: post-irradiation time; F_1: first filial generation; F_2: second filial generation; †: statistically significant for $p<0.05$, ††: statistically significant for $p<0.01$ (Student t-test).

Figure 2. The influence of cell cycle and DNA Damage Response (DDR) on the RAR. **(a)** Checkpoint assay of *Oregon*-R 0.4Gy LDR chronically exposed O*regon*-R larval brains versus non-treated (NT) controls. In the picture is shown the relative mitotic index (MI) calculated as the ratio between the MI of each irradiation treatment and the MI of NT *Oregon*-R wild type. Note that the relative MI of 0.4Gy LDR larvae increases after 60 minutes post-irradiation compared to NT control. At least three independent experiments were repeated. Values of $p<0.05$ (*) were considered as statistically significant (Student t-test). **(b)** EdU incorporation analysis of *Oregon*-R larval brain cells exposed to IR. EdU-positive cell nuclei of larval brains show 3 different incorporation patterns: S_1 represents early S phase nuclei that do not incorporate Edu in the DAPI-stained chromocenter; S_2 represents mid-S phase nuclei that incorporate EdU in all DAPI-stained nucleus; S_3 shows nuclei in the late S-phase that incorporate EdU only in the chromocenter. **(c)** Frequencies of EdU positive nuclei. The frequencies of EdU positive nuclei in each sample (NT, 0.4Gy LDR, 10Gy, 0.4Gy LDR + 10Gy) were obtained by examining at least 2000 nuclei from at least 2 brains. Values of $p<0.01$ (**) and $p<0.05$ (*) were considered as statistically significant (Student t-test). **(d)** Quantification (%) of EdU positive cells divided in S1, S2, and S3 phases according to the staining pattern observed in (b). No statistical differences were observed in treated cells compared to controls. **(e)** DNA repair gene mutant larvae do not elicit RAR. Frequency of CBs induced by an acute 2Gy, 5Gy or 10Gy irradiation on 0.4Gy LDR *Drosophila* strains mutated in genes involved in the DNA damage response (DDR). The *ATPCL* mutant was used as a control. Note that in all DNA repair (but not in

ATPCL) mutants RAR is abolished. ISOs: isochromosome deletions; CDs: chromatid deletions; CBs: chromosome breaks; NT: non-treated; PIR: post-irradiation time; †: $p<0.01$ (Student t-test). Bar= 10μm

Figure 3. DNA damage accumulation in 0.4Gy LDR -treated and non-treated larval brains.

(a) Anti γH2Av immunofluorescence on 10Gy irradiated cells showing (A) low damage (0-3 γH2Av spots per cell); (B) medium damage (4-7 γH2Av spots per cell); (C) high damage (> 7 γH2Av spots per cell **(b)** Quantification of γH2Av foci/cell at different PIR time points; non-pretreated (close circles) and 0.4Gy LDR -pretreated (open circles). Error bars represent the standard errors of the mean; lines only represent guide for the eye. Values of $p<0.01$ (**) and $p<0.05$ (*) were considered as statistically significant (Student t-test) **(c)** Western Blot analysis of γH2Av levels in treated and NT brains at 5 min, 15 min, 30 min, and 60 min PIR after acute IR exposure of 10Gy. Giotto (VIB) was used as a loading control. **(d)** Quantification of γH2Av signals from the WB analysis. Three independent WBs were used for the quantification. (*$p<0.05$; Student t-test); PIR: post-irradiation times. **(e)** Western Blot analysis of Nbs, Rad50, and Ku70 levels in treated and non-treated brains after 4 hours from acute IR exposure of 10Gy. Giotto (VIB) was used as a loading control. **(f)** Quantification of Nbs, Rad50, and Ku70 signals from the WB analysis. NT: non-treated. Bar= 10μm

Figure 4. Analysis of TFs frequency in telomere capping and DDR mutants exposed to 0.4Gy LDR.

(a) Examples of TFs scored for the TF frequency analysis. **(**A) Female wild-type metaphase; (B) female metaphase showing a Double Telomere Association (DTA) between the chromosomes 2 (arrows), a DTA involving both chromosomes 4 and both chromosomes X (arrows); (C) female metaphase showing a ring consisting of both X chromosomes (arrows) and a DTA between the chromosomes 4 (arrow); (D) female metaphase showing a multicentric chromosome configuration involving 3DTAs, a DTA between chromosome 4 and XR and a ring chromosome (arrows). **(b)** TF frequency (DTAs only) in 0.4Gy LDR-pretreated and non-treated *Drosophila* strains mutated in genes encoding DNA damage repair factors (*tefu*, *mre11*, *rad50*, and *nbs*), proteins of terminin complex (*cav*, and *ver*), or proteins not associated to terminin complex (*peo*, *eff*, and

Su(var)205). (**p*<0.05; ***p*<0.01). DTAs: double telomere associations; NT: non-treated. Bar= 5μm

Figure 5. Analysis of differentially expressed genes in radio adaptive response.
(a) Representation of the Venn diagram including all differentially expressed genes from 0.4Gy LDR + 10Gy *vs*. 10Gy (D *vs*. B), 0.4Gy LDR + 10Gy *vs*. 0.4Gy LDR (D *vs*. C) and 10Gy *vs*. 0.4Gy LDR (B *vs*. C) comparisons. Only a very low percentage of genes were in common among all comparisons. **(b)** Heat map representing the differentially expressed genes from 0.4Gy LDR + 10Gy *vs*. 10Gy (D *vs*. B) comparison belonging to "RNA processing" biological process obtained from DAVID functional enrichment analysis. The analysis was performed on three biological replicates obtained from three independent experiments, namely 2, 5, and 6. A color-coded scale for the normalized expression values is used: red and blue represent high and low expression levels. A complete list of differentially expressed genes is provided in the Supplementary Materials (Tables 3-7).

Figure 6. Loqs as a RAR responsive factor.
(a) RT-qPCR on different *Loqs* splicing variants and *mus308*. *Loqs-RD* (but not *-RB*, *-RA*, and *-RE*) transcripts are downregulated in 0.4Gy LDR exposed male brains following the exposure to 10Gy while *mus308* transcripts are upregulated. Three different experiments were performed. The statistical analysis used was Student t-test (**p*<0.05). **(b)** Different eye pigmentation in *GMR-w*^{IR} *Drosophila* flies exposed to 0.4Gy LDR+10Gy, 10Gy, and NT (non-treated). **(c)** Analysis of absorbance at 480 nm of eye pigmentation in NT, 0.4Gy LDR + 10Gy, and 10Gy treated flies. Student *t-test* was used for the statistical analysis *p<0.05* (*); NT: non-treated. **(d)** Frequency of IR-induced CBs in 0.4Gy LDR treated and non-treated (NT) homozygous and heterozygous *Loqs*^{KO} mutants as well as *OR*-R controls, in *loqs*^{KO} null mutants expressing the Loqs-PD and Loqs-PB exogenous isoforms. CBs: chromosome breaks; †: statistically significant using Student t-test (*p*<0.05). **(e)** Kinetics of γH2Av recruitment after irradiation with 10Gy in *loqs*^{KO} mutants; lines only represent guide for the eye. Student *t-test* (**p*<0.05) **(f)** The graph shows the TFs

a

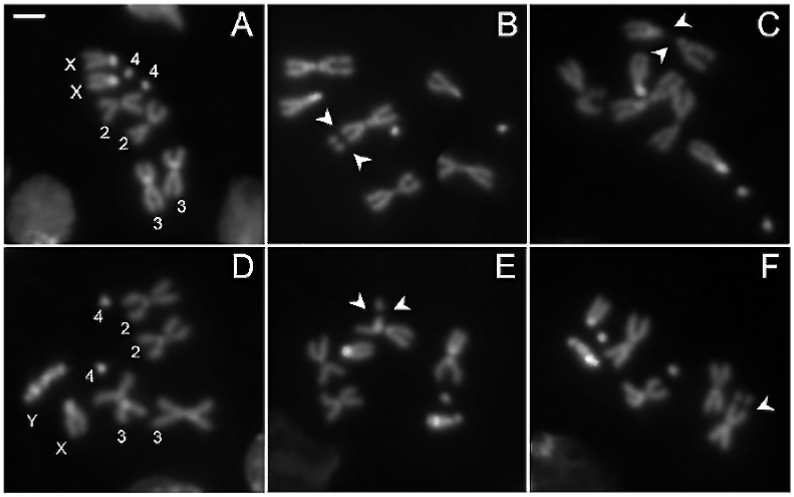

b

PIR	Sex	γ-ray treatment	Total cells scored	ISOs/ Cell	CDs/ Cell	CBs/ Cell
–	♀	NT	163	0.01±0.00	0.00±0.00	0.02±0.00
	♂	NT	154	0.01±0.00	0.00±0.00	0.02±0.00
	♀	0.4Gy	116	0.01±0.01	0.00±0.00	0.02±0.01
	♂	0.4Gy	140	0.02±0.02	0.00±0.00	0.04±0.02
4h	♀	10Gy	552	0.39±0.04	0.30±0.06	1.08±0.05
	♂	10Gy	409	0.33±0.02	0.16±0.02	0.82±0.06
	♀	0.4Gy + 10Gy	970	0.20±0.04†	0.20±0.02	0.60±0.02††
	♂	0.4Gy + 10Gy	418	0.16±0.02††	0.21±0.07	0.53±0.08††
8h	♀	10Gy	572	0.14±0.02	0.24±0.01	0.52±0.05
	♂	10Gy	236	0.16±0.05	0.23±0.01	0.55±0.10
	♀	0.4Gy + 10Gy	332	0.15±0.04	0.17±0.04	0.47±0.12
	♂	0.4Gy + 10Gy	334	0.14±0.04	0.15±0.02	0.42±0.10
F_1 4h	♀	10Gy	1157	0.19±0.02††	0.20±0.03	0.58±0.02††
	♂	10Gy	704	0.15±0.02††	0.16±0.05	0.46±0.03††
F_2 4h	♀	10Gy	423	0.25±0.02	0.39±0.04	0.89±0.05
	♂	10Gy	288	0.18±0.02	0.47±0.02	0.83±0.05

Figure 1

a

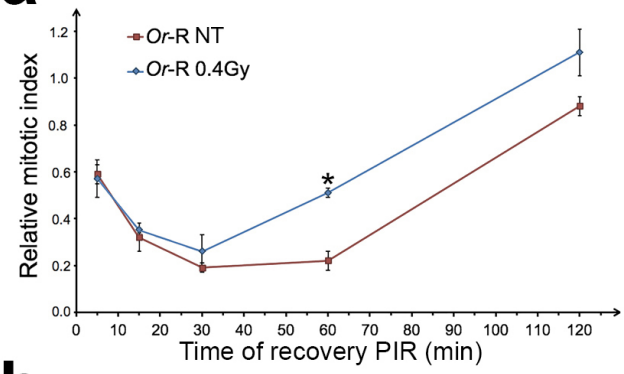

b

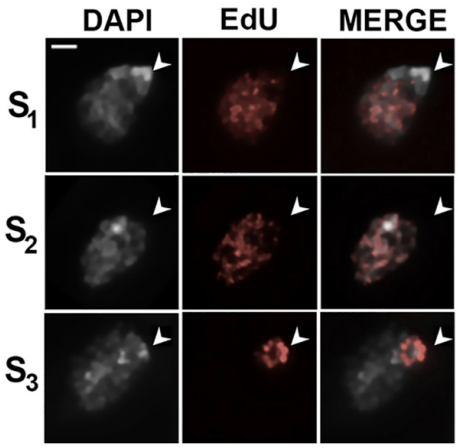

c

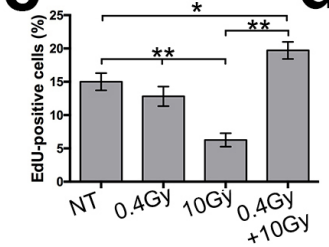

d

Nuclei %	S1	S2	S3
NT	51	33	14
0.4Gy	49	46	4
10Gy	48	46	4
0.4Gy + 10Gy	41	55	3

e

Genotype	γ-ray treatment	Total cells scored	CBs/ Cell
tefu^{atm6}	NT	194	0.11±0.02
	0.4Gy	251	0.12±0.05
	2Gy	278	0.88±0.15
	0.4Gy + 2Gy	233	0.70±0.07
mei41^{29D}*/ATR*	NT	290	0.08±0.03
	0.4Gy	613	0.11±0.01
	5Gy	227	1.26±0.09
	0.4Gy + 5Gy	304	1.52±0.18
mre11^{DC}	NT	208	0.33±0.06
	0.4Gy	229	0.31±0.03
	2Gy	325	1.11±0.12
	0.4Gy + 2Gy	296	0.86±0.07
rad50$^{\Delta 5.1}$	NT	218	0.12±0.01
	0.4Gy	208	0.17±0.03
	2Gy	244	1.87±0.16
	0.4Gy + 2Gy	151	1.83±0.09
nbs^{1}	NT	299	0.16±0.03
	0.4Gy	307	0.20±0.03
	2Gy	218	1.31±0.16
	0.4Gy + 2Gy	303	1.47±0.15
blm^{D3}	NT	70	0.05±0.01
	0.4Gy	60	0.06±0.02
	2Gy	37	1.17±0.13
	0.4Gy + 2Gy	74	1.04±0.07
rad51^{1}	NT	564	0.03±0.00
	0.4Gy	915	0.03±0.01
	10Gy	348	1.47±0.13
	0.4Gy + 10Gy	264	1.44±0.05
ku70	NT	150	0.03±0.01
	0.4Gy	120	0.05±0.01
	10Gy	300	1.23±0.06
	0.4Gy + 10Gy	124	1.09±0.03
ligIV^{5}	NT	197	0.30±0.04
	0.4Gy	179	0.27±0.04
	10Gy	491	0.98±0.15
	0.4Gy + 10Gy	569	0.76±0.08
ATPCL^{DG23}	NT	159	0.16±0.04
	0.4Gy	150	0.19±0.02
	10Gy	442	1.00±0.05
	0.4Gy + 10Gy	214	0.53±0.05†

Figure 2

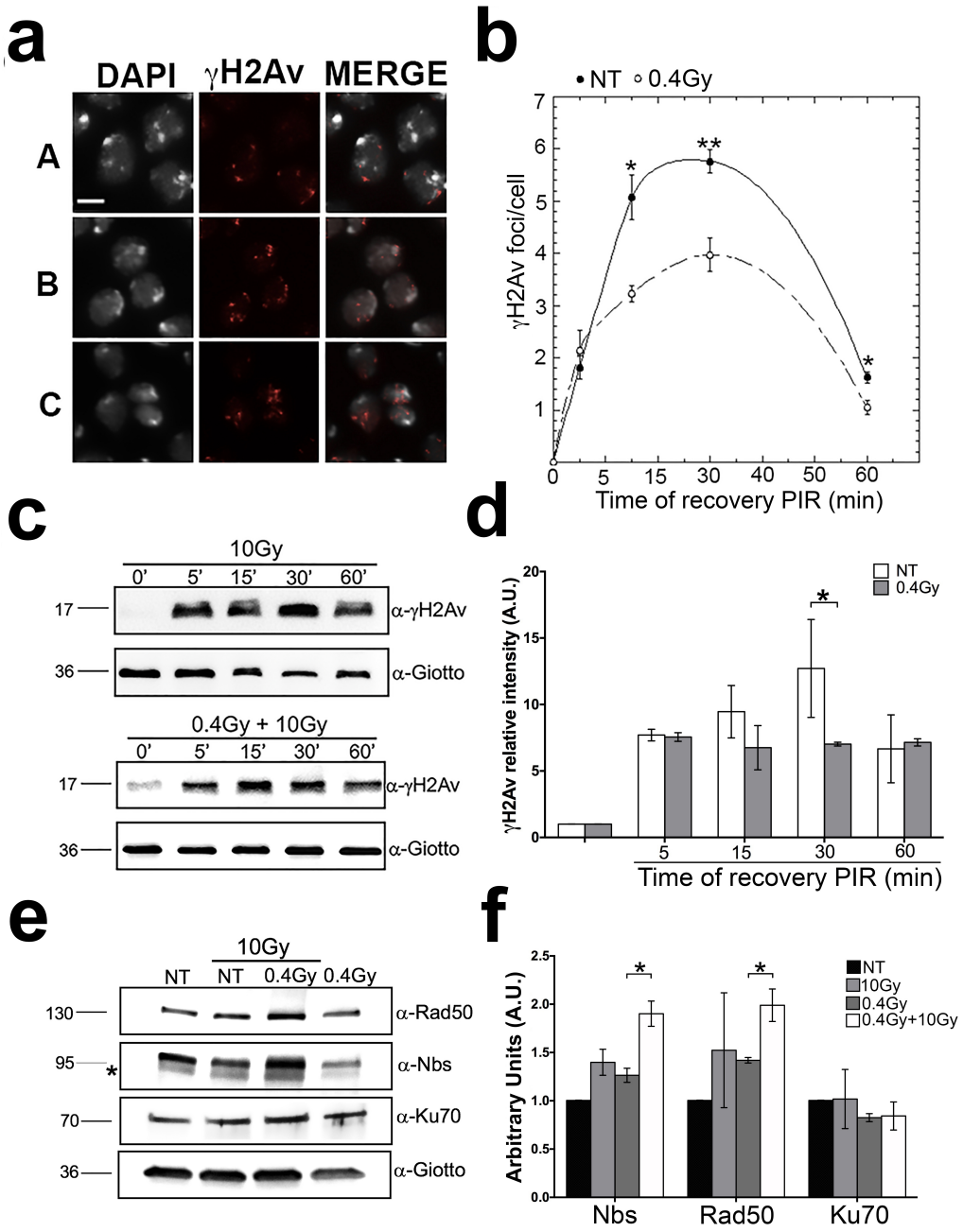
a
DAPI
γH2Av
MERGE
A
B
C
b
• NT ∘ 0.4Gy
γH2Av foci/cell
Time of recovery PIR (min)
c
10Gy
0' 5' 15' 30' 60'
17
36
α-γH2Av
α-Giotto
0.4Gy + 10Gy
0' 5' 15' 30' 60'
17
36
α-γH2Av
α-Giotto
d
NT
0.4Gy
γH2Av relative intensity (A.U.)
Time of recovery PIR (min)
e
10Gy
NT NT 0.4Gy 0.4Gy
130
95
70
36
α-Rad50
α-Nbs
α-Ku70
α-Giotto
f
NT
10Gy
0.4Gy
0.4Gy+10Gy
Arbitrary Units (A.U.)
Nbs
Rad50
Ku70

Figure 3

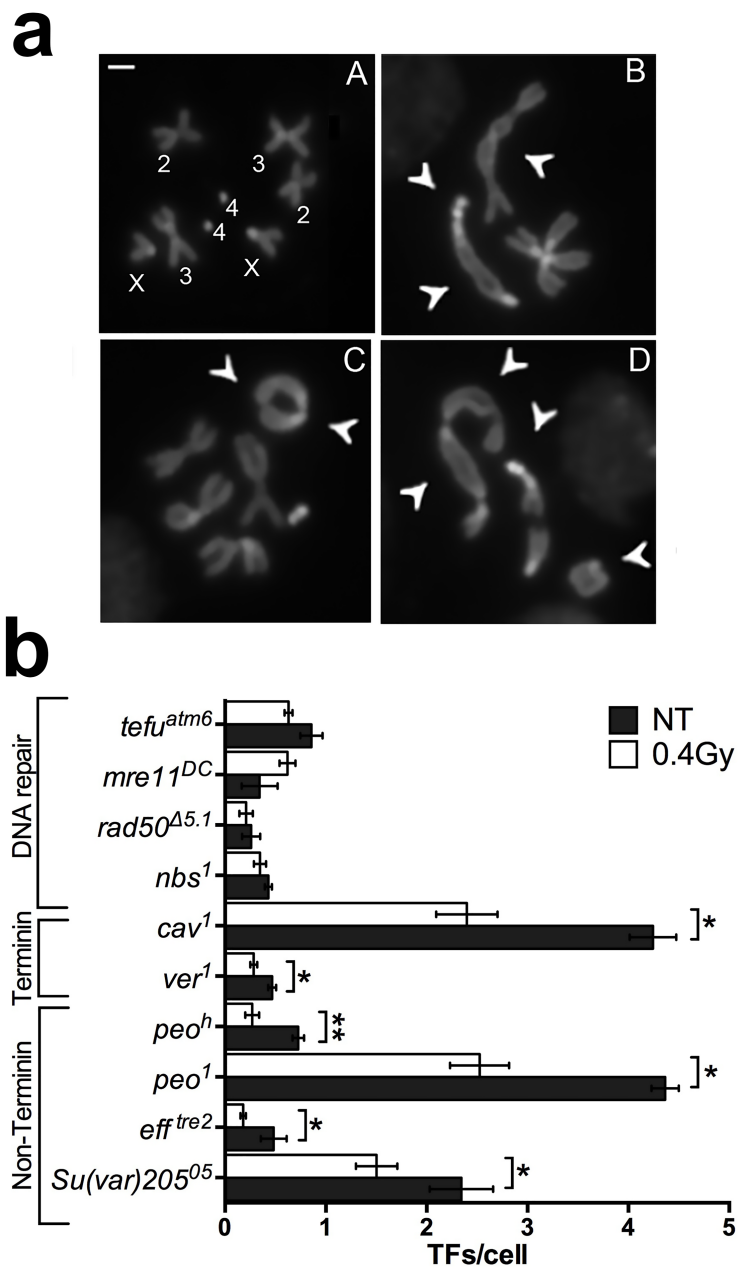
a
A
B
C
D
2
3
4
4
2
X
3
X
b
DNA repair
Terminin
Non-Terminin
tefu atm6
mre11 DC
rad50 Δ5.1
nbs 1
cav 1
ver 1
peo h
peo 1
eff tre2
Su(var)205 05
NT
0.4Gy
*
*
**
*
*
*
0
1
2
3
4
5
TFs/cell

Figure 4

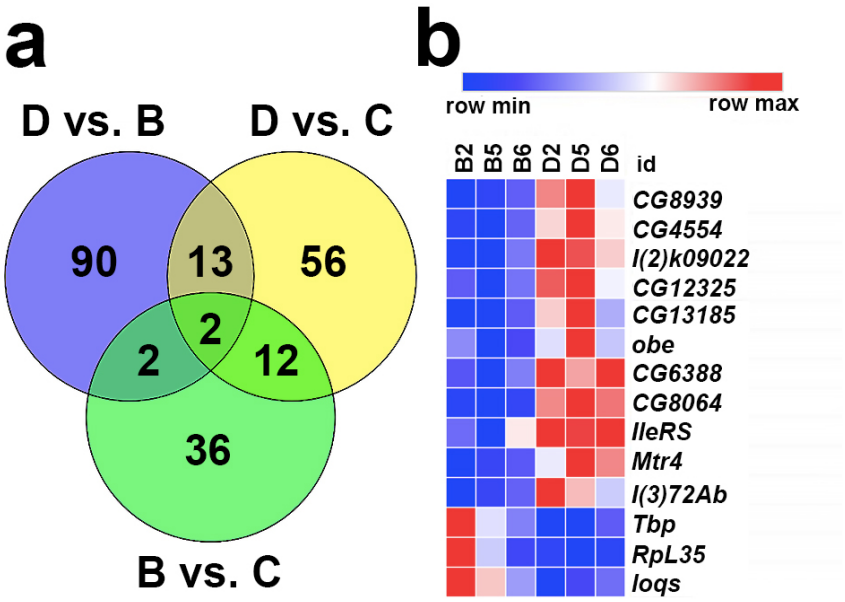
a
D vs. B
D vs. C
B vs. C
90
13
56
2
2
12
36
b
row min
row max
B2
B5
B6
D2
D5
D6
id
CG8939
CG4554
l(2)k09022
CG12325
CG13185
obe
CG6388
CG8064
IleRS
Mtr4
l(3)72Ab
Tbp
RpL35
loqs

Figure 5

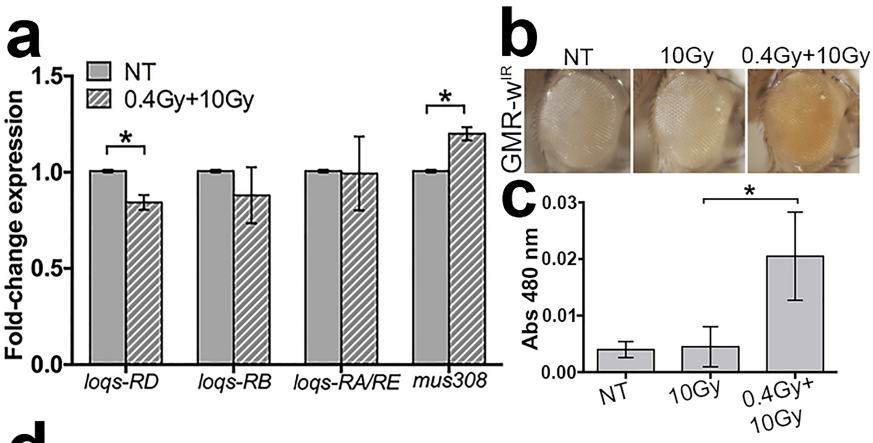

d

Genotype	γ-ray treatment	Total cells scored	CBs/ Cell
Or-R	10Gy	961	0.96±0.04
loqs^{KO} /loqs^{KO}	NT	497	0.03±0.01
	0.4Gy	339	0.03±0.01
	10Gy	561	0.40±0.05††
	0.4Gy + 10Gy	679	0.59±0.11†
loqs^{KO}/+	10Gy	211	0.53±0.12†
	0.4Gy + 10Gy	305	0.56±0.06††
loqs^{KO};[loqs-PD]	10Gy	175	1.13±0.16
loqs^{KO};[loqs-PB]	10Gy	133	0.54±0.07††

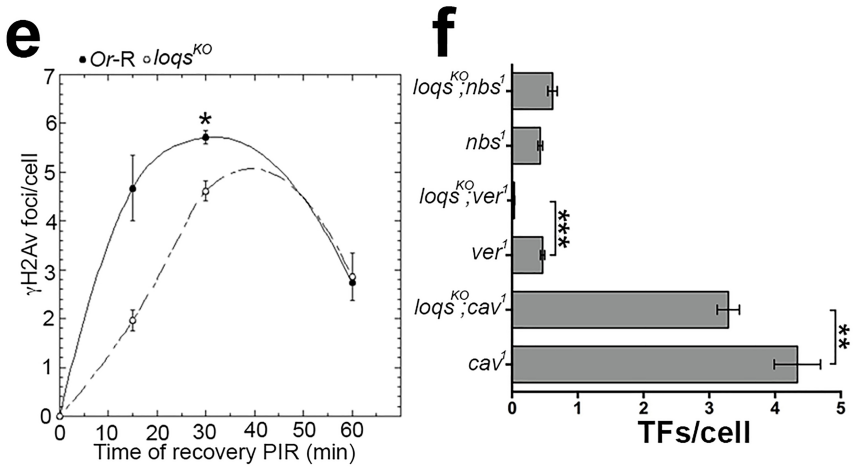

Figure 6

Supplementary Table 1. Frequency of chromosome breaks observed in F_1 and F_2 generations from 0.4Gy LDR-treated parents.

Generation[a]	Total cells scored	ISOs/ Cell	CDs/ Cell	CBs/ Cell
P	680	0.35±0.02	0.24±0.02	0.94±0.04
F_1 from ♀^{T}X♂^{NT}	291	0.35±0.03	0.25±0.03	0.95±0.06
F_1 from ♀^{NT} X♂^{T}	254	0.35±0.04	0.29±0.03	0.99±0.06

The table shows the quantification of CBs in F_1 and F_2 generations obtained from *Oregon-R* parents exposed, during their embryo-third instar larvae transition, to a 0.4Gy LDR γ-ray treatment. Following the 10Gy acute exposure, it is possible to notice a maintaining of CBs frequency reduction in F_1 but not in F_2 (transgenerational effect). The total frequency of CBs was calculated considering the ISOs as 2 breaks and the CBs as 1. Eventual chromosome exchanges were not considered into the analysis. The CBs frequencies were obtained by examining for each condition at least 200 nuclei from 3 brains. The statistical analysis was performed using the t-Student Test. a= Third instar larvae exposed to a 10Gy *challenge* dose have been analyzed for each generation; P: parental generation; F_1: first filial generation; F_2: second filial generation; T: treated; NT: non-treated; ISOs: isochromosome deletions; CD: chromatid deletions; CBs: chromosome breaks.

Supplementary Table 2. Frequency of chromosome breaks observed in *nbs^1* single mutants and *loqs^{KO};nbs^1* double mutants.

Genotype	γ-ray treatment	Total cells scored	CBs/ Cell
nbs^1	NT	299	0.15
	2Gy	156	1.11
loqs^{KO} /+; nbs^1/+	NT	84	0.01
	2Gy	122	0.41
loqs^{KO} /+; nbs^1/ nbs^1	NT	282	0.26
	2Gy	38	1.84
loqs^{KO} / loqs^{KO}; nbs^1/+	NT	139	0.03
	2Gy	32	0.60
loqs^{KO} / loqs^{KO}; nbs^1/ nbs^1	NT	317	0.23
	2Gy	22	1.95

The table shows the frequency of IR-induced CBs in *nbs^1* single mutant and *loqs;nbs^1* double mutants. The statistical analysis performed was the Student t-test. CBs: chromosome breaks.

Supplementary Figure 1. The experimental set up.

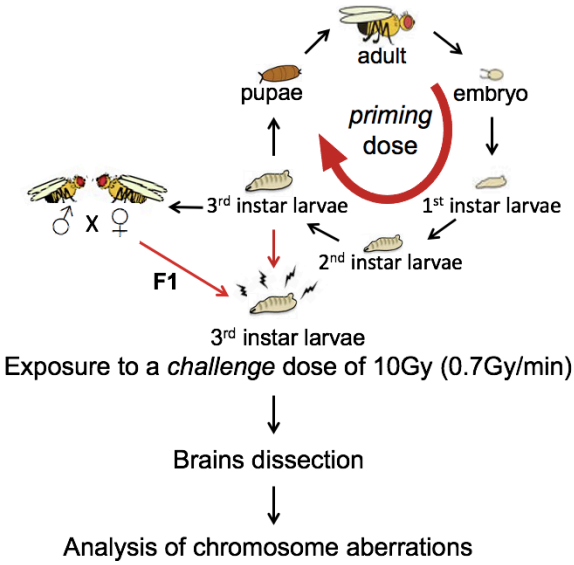

The *priming* dose of 0.4Gy (LDR) was delivered with a dose-rate of 2.5mGy/h during the embryos-larvae transition. The third instar larvae were collected and exposed to the *challenge* dose of 10Gy delivered with a dose-rate of 0.7Gy/min. After that, the brains were dissected to analyze the Chromosome aberrations frequency. Males and females pretreated (0.4Gy LDR) during their development were crossed to obtain F_1. The third instar F_1 larvae were exposed to the *challenge* dose of 10Gy to analyze the Chromosome aberrations frequency.

Supplementary Figure 2. The prolonged exposure of *Oregon*-R to a 0.2Gy (1.2mGy/h) does not reduce the frequency of CBs and the expression of *Loqs*-RD transcript.

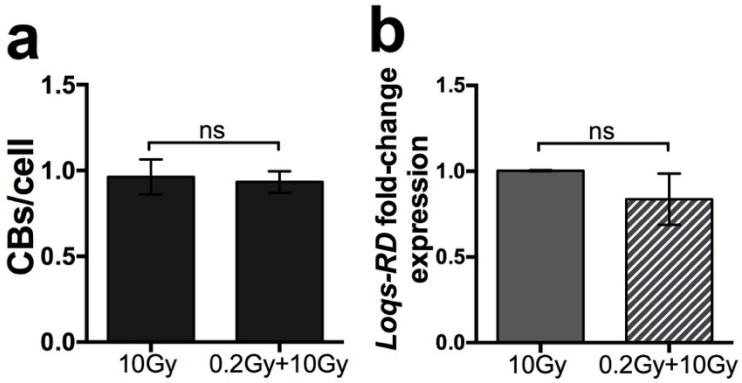

(a) Frequencies of CBs observed in *Oregon*-R Drosophila strains treated during their development until the reaching of the third instar larvae stage with a low dose of 0.2Gy at a dose-rate of 1.2mGy/h and non-treated controls after the exposure to the *challenging* dose of 10Gy**.** CBs: chromosome breaks; ns: no significant. At least three independent experiments were conducted, and 200 cells were analyzed. The statistical analysis was assessed using the Student t-test. **(b)** RT-qPCR of Loqs-RD performed in samples chronically exposed to a low dose of 0.2Gy and then treated with 10Gy versus samples exposed to 10Gy alone. The statistical analysis was conducted using the Student *t-test*; ns: not significant.

Supplementary Figure 3. Apoptosis analysis in irradiated larval brains and wing imaginal discs.

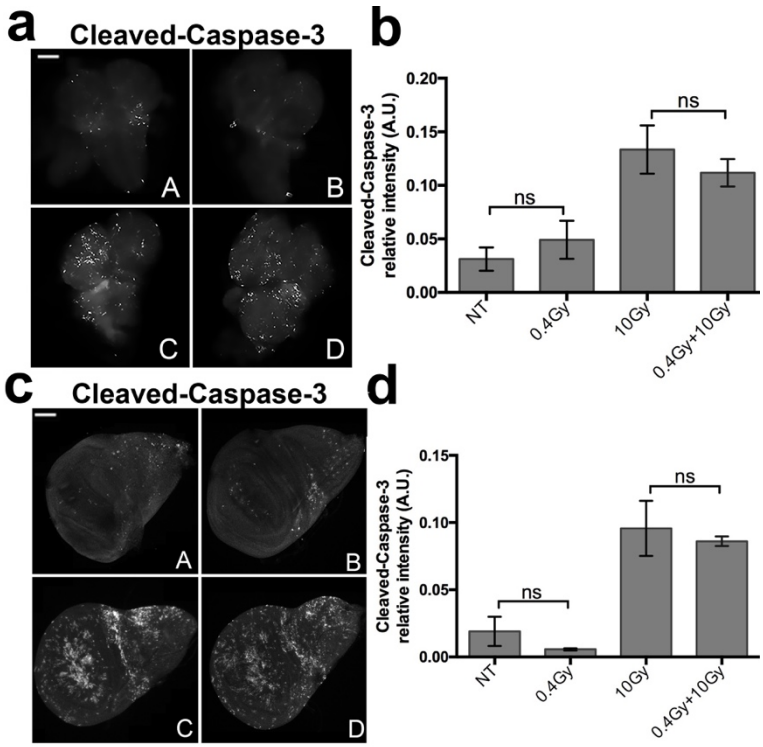

(a) Immunofluorescence with anti-cleaved-caspase-3 on larval brains; (A, C) Untreated and (B, D) 0.4Gy LDR disc after exposure to 10Gy. **(b)** Quantification of Cleaved-Caspase-3 signals; ns: no statistically significant values; NT: non-treated. **(c)** Immunofluorescence with anti-cleaved-caspase-3 on wing imaginal discs; (A, C) Untreated and (B, D) 0.4Gy LDR disc after exposure to 10Gy. **(d)** Quantification of Cleaved-Caspase-3 signals; ns: no statistically significant values; NT: non-treated.

Supplementary Figure 4. Telomeric γH2Av foci analysis and Het-A expression in 0.4Gy LDR telomere capping mutants.

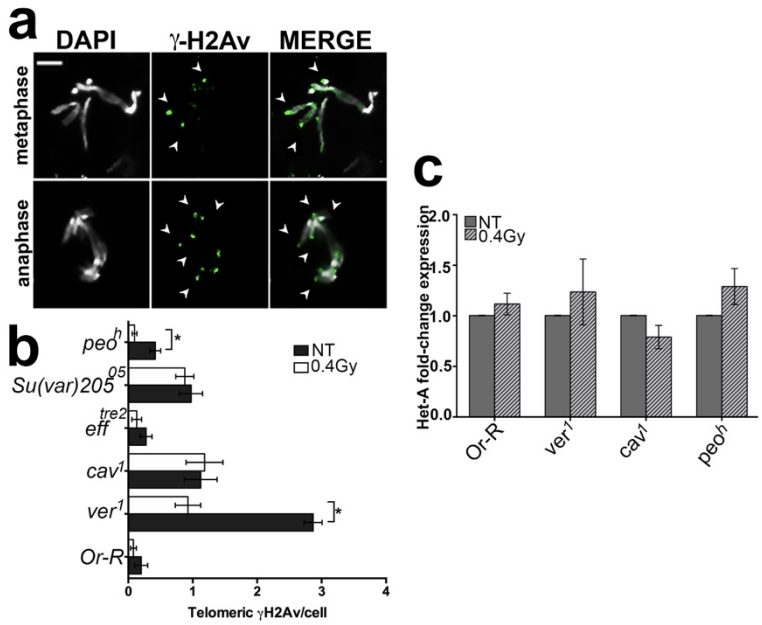

(a). Examples of γH2Av localization (green) on chromosome ends (arrows) from a mutant metaphase and anaphase. **(b)** Frequency of Telomeric γH2Av foci in 0.4Gy LDR telomere capping mutants. Student t-test (*p<0.05); NT: non-treated. **(c)** Het-A expression in 0.4Gy LDR and untreated *Or*-R, *ver*^{1}, *cav*^{1}, and *peo*^{h} third instar larvae. The qPCR shows no statistically significative differences between the 0.4Gy LDR-treated samples and the corresponding untreated controls. Student t-test (p<0.05); NT: non-treated.

Supplementary figure 5. 0.4Gy-LDR ionizing radiation doses do not affect *Oregon*-R life span and fertility.

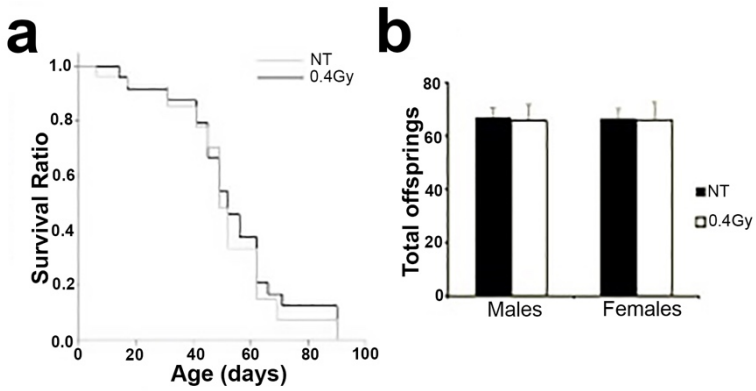

(a) Life span Kaplan-Meier analysis of *Oregon*-R males treated (0.4Gy LDR, black line) and non-treated (NT, gray line). The survival ratio is indistinguishable in the two samples. Long-rank: 0.249; p=0.618. **(b)** The low dose exposure does not influence the male and female fertility. In the graph are represented the average number of individuals born from three different crosses. NT: non-treated.

References

1 UNSCEAR. Sources and Effects of Ionizing Radiation: United Nations 2008.

2 Morgan WF, Bair WJ. Issues in low dose radiation biology: the controversy continues. A perspective. *Radiat Res* 2013; **179**:501-510.

3 Shibamoto Y, Nakamura H. Overview of Biological, Epidemiological, and Clinical Evidence of Radiation Hormesis. *Int J Mol Sci* 2018; **19**.

4 Council NR. Health Risks from Exposure to Low Levels of Ionizing Radiation: BEIR VII Phase 2. Washington, DC: The National Academies Press 2006.

5 Marcus CS. Destroying the Linear No-threshold Basis for Radiation Regulation: A Commentary. *Dose Response* 2016; **14**:1559325816673491.

6 Calabrese EJ. The Mistaken Birth and Adoption of LNT: An Abridged Version. *Dose Response* 2017; **15**:1559325817735478.

7 Calabrese EJ. On the origins of the linear no-threshold (LNT) dogma by means of untruths, artful dodges and blind faith. *Environ Res* 2015; **142**:432-442.

8 Belli M, Tabocchini MA. Ionizing Radiation-Induced Epigenetic Modifications and Their Relevance to Radiation Protection. *Int J Mol Sci* 2020; **21**.

9 Esposito G, Campa A, Pinto M, Simone G, Tabocchini MA, Belli M. Adaptive response: modelling and experimental studies. *Radiation protection dosimetry* 2011; **143**:320-324.

10 Nenoi M, Wang B, Vares G. In vivo radioadaptive response: a review of studies relevant to radiation-induced cancer risk. *Human & experimental toxicology* 2015; **34**:272-283.

11 Tapio S, Jacob V. Radioadaptive response revisited. *Radiation and environmental biophysics* 2007; **46**:1-12.

12 Olivieri G, Bodycote J, Wolff S. Adaptive response of human lymphocytes to low concentrations of radioactive thymidine. *Science* 1984; **223**:594-597.

13 Stecca C, Gerber GB. Adaptive response to DNA-damaging agents: a review of potential mechanisms. *Biochemical pharmacology* 1998; **55**:941-951.

14 Lustig A, Shterev I, Geyer S *et al.* Long term effects of radiation exposure on telomere lengths of leukocytes and its associated biomarkers among atomic-bomb survivors. *Oncotarget* 2016; **7**:38988-38998.

15 Luxton JJ, McKenna MJ, Taylor LE *et al.* Temporal Telomere and DNA Damage Responses in the Space Radiation Environment. *Cell Rep* 2020; **33**:108435.

16 Luxton JJ, McKenna MJ, Lewis A *et al.* Telomere Length Dynamics and DNA Damage Responses Associated with Long-Duration Spaceflight. *Cell Rep* 2020; **33**:108457.

17 Das B, Saini D, Seshadri M. Telomere length in human adults and high level natural background radiation. *PLoS One* 2009; **4**:e8440.

18 Movahedi A, Mostajaboddavati M, Rajabibazl M, Mirfakhraie R, Enferadi M. Association of telomere length with chronic exposure to ionizing radiation among inhabitants of natural high background radiation areas of Ramsar, Iran. *Int J Radiat Biol* 2019; **95**:1113-1121.

19 Esposito G, Anello P, Pecchia I, Tabocchini MA, Campa A. Facility for gamma irradiations of cultured cells at low dose rates: design, physical characteristics and functioning. *Appl Radiat Isot* 2016; **115**:227-234.

20 Gatti M, Tanzarella C, Olivieri G. Analysis of the chromosome aberrations induced by x-rays in somatic cells of Drosophila melanogaster. *Genetics* 1974; **77**:701-719.

21 Hart T, Tong AHY, Chan K *et al.* Evaluation and Design of Genome-Wide CRISPR/SpCas9 Knockout Screens. *G3 (Bethesda)* 2017; **7**:2719-2727.

22 Cenci G, Ciapponi L, Marzullo M *et al.* The Analysis of Pendolino (peo) Mutants Reveals Differences in the Fusigenic Potential among Drosophila Telomeres. *PLoS Genet* 2015; **11**:e1005260.

23 Madigan JP, Chotkowski HL, Glaser RL. DNA double-strand break-induced phosphorylation of Drosophila histone variant H2Av helps prevent radiation-induced apoptosis. *Nucleic Acids Res* 2002; **30**:3698-3705.
24 Raffa GD, Ciapponi L, Cenci G, Gatti M. Terminin: a protein complex that mediates epigenetic maintenance of Drosophila telomeres. *Nucleus* 2011; **2**:383-391.
25 Cacchione S, Cenci G, Raffa GD. Silence at the End: How Drosophila Regulates Expression and Transposition of Telomeric Retroelements. *J Mol Biol* 2020; **432**:4305-4321.
26 Cipressa F, Cenci G. DNA damage response, checkpoint activation and dysfunctional telomeres: face to face between mammalian cells and Drosophila. *Tsitologiia* 2013; **55**:211-217.
27 Cenci G. Drosophila cell cycle under arrest: uncapped telomeres plead guilty. *Cell Cycle* 2009; **8**:990-995.
28 Korandova M, Krucek T, Szakosova K *et al.* Chronic low-dose pro-oxidant treatment stimulates transcriptional activity of telomeric retroelements and increases telomere length in Drosophila. *J Insect Physiol* 2018; **104**:1-8.
29 Marques JT, Kim K, Wu PH, Alleyne TM, Jafari N, Carthew RW. Loqs and R2D2 act sequentially in the siRNA pathway in Drosophila. *Nat Struct Mol Biol* 2010; **17**:24-30.
30 Zhou R, Czech B, Brennecke J *et al.* Processing of Drosophila endo-siRNAs depends on a specific Loquacious isoform. *RNA* 2009; **15**:1886-1895.
31 Lim MY, Ng AW, Chou Y *et al.* The Drosophila Dicer-1 Partner Loquacious Enhances miRNA Processing from Hairpins with Unstable Structures at the Dicing Site. *Cell Rep* 2016; **15**:1795-1808.
32 Hartig JV, Esslinger S, Bottcher R, Saito K, Forstemann K. Endo-siRNAs depend on a new isoform of loquacious and target artificially introduced, high-copy sequences. *EMBO J* 2009; **28**:2932-2944.
33 Saito K, Ishizuka A, Siomi H, Siomi MC. Processing of pre-microRNAs by the Dicer-1-Loquacious complex in Drosophila cells. *PLoS Biol* 2005; **3**:e235.
34 Okamura K, Chung WJ, Ruby JG, Guo H, Bartel DP, Lai EC. The Drosophila hairpin RNA pathway generates endogenous short interfering RNAs. *Nature* 2008; **453**:803-806.
35 Lee YS, Carthew RW. Making a better RNAi vector for Drosophila: use of intron spacers. *Methods* 2003; **30**:322-329.
36 Panier S, Boulton SJ. Double-strand break repair: 53BP1 comes into focus. *Nat Rev Mol Cell Biol* 2014; **15**:7-18.
37 Cenci G, Ciapponi L, Gatti M. The mechanism of telomere protection: a comparison between Drosophila and humans. *Chromosoma* 2005; **114**:135-145.
38 Doksani Y, de Lange T. The role of double-strand break repair pathways at functional and dysfunctional telomeres. *Cold Spring Harb Perspect Biol* 2014; **6**:a016576.
39 Slijepcevic P. The role of DNA damage response proteins at telomeres--an "integrative" model. *DNA Repair (Amst)* 2006; **5**:1299-1306.
40 Verdun RE, Karlseder J. The DNA damage machinery and homologous recombination pathway act consecutively to protect human telomeres. *Cell* 2006; **127**:709-720.
41 Bosso G, Cipressa F, Moroni ML *et al.* NBS1 interacts with HP1 to ensure genome integrity. *Cell Death Dis* 2019; **10**:951.
42 On K, Crevel G, Cotterill S, Itoh M, Kato Y. Drosophila telomere capping protein HOAP interacts with DSB sensor proteins Mre11 and Nbs. *Genes Cells* 2021.
43 Fukunaga R, Han BW, Hung JH, Xu J, Weng Z, Zamore PD. Dicer Partner Proteins Tune the Length of Mature miRNAs in Flies and Mammals. *Cell* 2012; **151**:912.
44 Marques JT, Wang JP, Wang X *et al.* Functional specialization of the small interfering RNA pathway in response to virus infection. *PLoS Pathog* 2013; **9**:e1003579.

45 Francia S, Michelini F, Saxena A *et al.* Site-specific DICER and DROSHA RNA products control the DNA-damage response. *Nature* 2012; **488**:231-235.
46 Wei W, Ba Z, Gao M *et al.* A role for small RNAs in DNA double-strand break repair. *Cell* 2012; **149**:101-112.
47 Michalik KM, Bottcher R, Forstemann K. A small RNA response at DNA ends in Drosophila. *Nucleic Acids Res* 2012; **40**:9596-9603.
48 Gao M, Wei W, Li MM *et al.* Ago2 facilitates Rad51 recruitment and DNA double-strand break repair by homologous recombination. *Cell Res* 2014; **24**:532-541.
49 Malone CD, Hannon GJ. Small RNAs as guardians of the genome. *Cell* 2009; **136**:656-668.
50 Laurencon A, Purdy A, Sekelsky J, Hawley RS, Su TT. Phenotypic analysis of separation-of-function alleles of MEI-41, Drosophila ATM/ATR. *Genetics* 2003; **164**:589-601.
51 Silva E, Tiong S, Pedersen M *et al.* ATM is required for telomere maintenance and chromosome stability during Drosophila development. *Curr Biol* 2004; **14**:1341-1347.
52 Ciapponi L, Cenci G, Ducau J *et al.* The Drosophila Mre11/Rad50 complex is required to prevent both telomeric fusion and chromosome breakage. *Curr Biol* 2004; **14**:1360-1366.
53 Ciapponi L, Cenci G, Gatti M. The Drosophila Nbs protein functions in multiple pathways for the maintenance of genome stability. *Genetics* 2006; **173**:1447-1454.
54 Raffa GD, Raimondo D, Sorino C *et al.* Verrocchio, a Drosophila OB fold-containing protein, is a component of the terminin telomere-capping complex. *Genes Dev* 2010; **24**:1596-1601.
55 Raffa GD, Siriaco G, Cugusi S *et al.* The Drosophila modigliani (moi) gene encodes a HOAP-interacting protein required for telomere protection. *Proc Natl Acad Sci U S A* 2009; **106**:2271-2276.
56 Cenci G, Rawson RB, Belloni G *et al.* UbcD1, a Drosophila ubiquitin-conjugating enzyme required for proper telomere behavior. *Genes Dev* 1997; **11**:863-875.
57 Cenci G, Siriaco G, Raffa GD, Kellum R, Gatti M. The Drosophila HOAP protein is required for telomere capping. *Nat Cell Biol* 2003; **5**:82-84.
58 Cipressa F, Romano S, Centonze S *et al.* Effete, a Drosophila chromatin-associated ubiquitin-conjugating enzyme that affects telomeric and heterochromatic position effect variegation. *Genetics* 2013; **195**:147-158.
59 Giansanti MG, Bonaccorsi S, Kurek R *et al.* The class I PITP giotto is required for Drosophila cytokinesis. *Curr Biol* 2006; **16**:195-201.
60 Huang da W, Sherman BT, Lempicki RA. Systematic and integrative analysis of large gene lists using DAVID bioinformatics resources. *Nat Protoc* 2009; **4**:44-57.